EXPLORATION OF A SUBSURFACE STRUCTURE MODEL IN A WIDE DEPTH RANGE USING EARTHQUAKE MOTIONS ON THE SURFACE

K. Motoki[(1)], and K. Kato[(2)]

[(1)] *Senior Manager, Kobori Research Complex, kmoto@kobori-takken.co.jp*
[(2)] *Managing Director, Kobori Research Complex, katokenichi@kobori-rc.com*

Abstract

Subsurface structure models for earthquake motion prediction are often evaluated by PS logging, microtremor exploration and/or other explorations. However, PS logging may not be applicable everywhere due to economic factors, and microtremor exploration may not be always applicable because the topographical and geological interfaces may not be approximated by surface wave theory. When such geophysical exploration is difficult to apply, it is desirable to make a subsurface structure model using earthquake motion records or, preferably, with simpler observations, for example, a single observation only on the ground surface.

We have two methods for estimating a subsurface structure model from earthquake motion records on the surface: horizontal-to-vertical spectral ratio (HVSR) on diffuse wavefield theory and receiver function (RF). The HVSR technique is based on the theory of body waves, and the accuracy of the subsurface structure model derived from the short period range is greater than that from the long period range in which the surface waves are dominant. RF is based on the theory of PS converted waves, and the accuracy of the model derived from the long period range is greater than that from the short period range in which the incidence and converted waves are contaminated by scattering. If we can make use of a complementary combination of the high accurate period ranges, we can construct a sufficient model from earthquake motion records only on the surface, by means of a joint inversion of HVSR and RF.

We applied the inversion method to CHBH04, where the depth of the seismic bedrock is approximately 1.5 km and the predominant period is evaluated as approximately 8 s. We used a hybrid heuristic method of genetic algorithms and simulated annealing as the inversion procedure. For the combination of HVSR and RF, the error function was set as the sum of each error function of HVSR and RF, multiplied by the contribution weights. The contribution weights of HVSR–RF were set to 50–50 for the joint inversion, and 0–100 and 100–0 for the single inversions, to examine the effect of the joint inversion.

According to the results of the joint inversion and the RF and HVSR single inversions, it can be said that the model in which HVSR and RF are simultaneously used reflects the high sensitivity in a wider depth range than that of each individual inversion. However, both HVSR and RF present a problem in that it is difficult to uniquely estimate the S wave velocity and the thickness of the intermediate layer because of a trade-off between them; the trade-off could not be solved even by the joint inversion. To improve their accuracy, other physical quantities for an inversion, or *a priori* information, e.g., the depth of soil layer boundary by excavation, are necessary.

Keywords: diffuse wave field theory; horizontal-to-vertical spectral ratio; receiver function; joint inversion

1. Introduction

To make a subsurface structure model for earthquake motion prediction, the field of geophysics has various methods of exploration. We have often adopted PS logging and microtremor exploration. PS logging may not be applicable everywhere due to economic factors, and microtremor exploration may not be always applicable because the topographical and geological interfaces may not be approximated by surface wave theory. When such geophysical exploration is difficult to apply, it is desirable to make a subsurface structure model using earthquake motion records or, preferably, with simpler observations, for example, a single observation only on the ground surface.

We have two methods for estimating a subsurface structure model from earthquake motion records on the ground surface: horizontal-to-vertical spectral ratio of earthquake motions on diffuse wavefield theory (HVSR) (proposed by Kawase et al. [1]) and receiver function (RF) (proposed by Langston, 1979 [2]). The HVSR technique is based on the theory of body waves, and the accuracy of the subsurface structure model derived from the short period range is greater than that from the long period range in which the surface waves are dominant. RF is based on the theory of PS converted waves, and the accuracy of the model derived from the long period range is greater than that from the short period range in which the incidence and converted waves are contaminated by scattering. If we can make use of a complementary combination of the high accurate period ranges, we can construct a sufficient model from the earthquake motion records only on the surface by means of a joint inversion of HVSR and RF. The subsurface model inversion was applied to KiK-net stations, and the validity of the model was estimated with the earthquake motions observed at ground level and down hole. We also used a PS logging model obtained from a previous study as one of the subsurface models in this validation.

2. Method

We used HVSR and RF for an estimation of the subsurface models. We first performed a simple sensitivity test using various subsurface models to compare the sensitivity of HVSR with that of RF for the shallow and deep parts of the surface structure. Figure 1 shows the models used in this test and the theoretical values of HVSR and RF. Model 1, drawn by the blue line in Fig. 1(A), was used as the reference model, and we set model 2 (drawn by the green line) with varying deep parts of the model and model 3 (drawn by the red line) with varying shallow parts of the model. The right panel of Fig. 1(A) does not show any deeper than GL-20 m because we set the deeper part in model 3 to be the same as that in model 1.

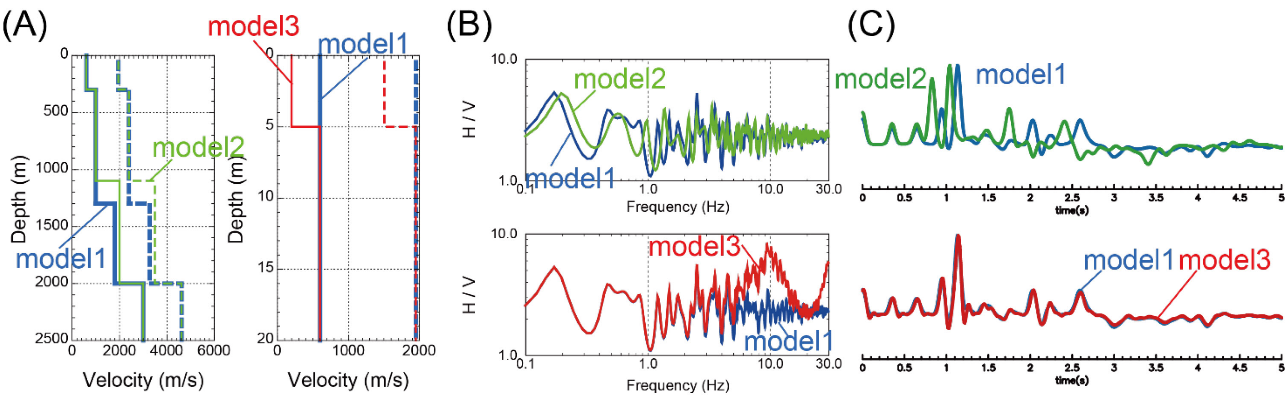

Fig. 1 – (A) Vs and Vp profiles of the subsurface models for sensitivity analysis (basic model: model 1, deep section changed: model 2, and shallow section changed: model 3), (B) HVSR variations when changing the shallow and deep parts of the subsurface models, and (C) RF variations when changing the models similarly to (B).

When the deep part was varied (as in the upper panels in Fig. 1(B) and (C)), the difference in the HVSRs between model 1 and model 2 was inconspicuous, but the difference in RFs could be clearly found. On the other hand, when the shallow part was varied (as in the lower panels in Fig. 1(B) and (C)), there was a large difference in the HVSRs of model 1 and model 3 of approximately 10 Hz but almost no difference in the RFs. In other words, it is expected that the RF has high sensitivity to the deep part of the subsurface models and that HVSR has high sensitivity to the shallow part of the models.

We adopted the hybrid heuristic method proposed by Yamanaka (2007) [3] for an inversion scheme. This method combines genetic algorithms and simulated annealing and does not require an initial value. In addition, this method has an advantage in that it can search the neighborhood of the global minimum without falling into the local minimum. The number of individuals was set to 100, the maximum number of generations was set to 1,000, and 10 sets were created by changing the random number of the initial value of the set. Among the models searched in the 10 sets, we picked the model that gave the minimum error as the final estimated subsurface model. The function of the overall error is as shown in the following equation (to adjust the dimensions in HVSR and RF, each error was divided by the standard deviation):

$$\varphi = p\varphi_{HV} + (1-p)\varphi_{RF}, \tag{1}$$

$$\varphi_{HV} = \sqrt{\frac{1}{N_{HV}}\sum \frac{|log\, HV_{obs}(\omega) - log\, HV_{cal}(\omega)|^2}{\sigma\{log\, HV_{obs}(\omega)\}^2}}, \tag{2}$$

$$\varphi_{RF} = \frac{1}{N_{RF}}\sum \frac{|RF_{obs}(t) - RF_{cal}(t)|}{\sigma\{RF_{obs}(t)\}}, \tag{3}$$

where p is a weight of HVSR in the inversion, HV_{obs} is the observed HVSR, HV_{cal} is the calculated HVSR, and N_{HV} is the number of earthquakes for the HVSR. RF_{obs} is the observed RF, RF_{cal} is the calculated RF, and N_{RF} is the number of earthquakes for the RF. We set the values of p to 0, 0.5, and 1, and we performed each individual inversion when 0 was set to 0 and 1 and the joint inversion when p was set to 0.5. The purpose of performing the individual inversions was to examine the effect of the joint inversion. We referred the PS logging model to be compared; this has been investigated by Ohta et al. (1980) [4] and Kinoshita and Ohike (2002) [5]. Because both the HVSR and RF have low sensitivity to the damping factor, we independently evaluated the damping factor before the inversions using a seismic interferometry technique (Fukushima et al., 2016 [6]), and we set the damping factor of waves to 1% in the following inversions; the simulation is described in section 5.

3. Test Site and Observed HVSR and RF

We chose CHBH04, which had a thick sedimentary layer, as a test site. At the station, an accelerometer was installed at GL-2300 m, as well as at the ground surface. For the earthquake selection, we imposed conditions that earthquakes used for an evaluation of HVSR would dominate body waves and that earthquakes used for an evaluation of RF would be sufficiently oblique in the incident P wave to generate a PS converted wave. For HVSR, we selected 768 earthquakes under the five conditions: 1) occurred before the main shock, 2) depths were ≤100 km, 3) hypocentral distances were <200 km, 4) hypocentral distance to depth ratios were <2, and 5) PGA was <100 cm/s^2. For RF, we selected 58 earthquakes under the five conditions: 1) occurred before the main shock, 2) depths were ≤50 km, 3) hypocentral distances were >150 and <500 km, 4) the P wave appeared 2 s after the start of recording, and 5) PGA was <100 cm/s^2.

The epicenters of the selected earthquakes and the station are shown in Fig. 2. For the evaluation of HVSRs, we used a 40 s part of the S wave. The arrival time of the S wave was determined by subtracting 1 s from the evaluated time with reference to the S wave travel time obtained from the JMA travel time table (Ueno et al., 2002 [7]). The Fourier amplitude was smoothed with a Parzen window with a bandwidth of

0.05 Hz. The average value of HVSR for the selected earthquakes was used as the observed HVSR. The evaluation result is shown in Fig. 3(A). We extracted data used in the inversions so that the resultant frequency almost equally divided into 100 points along a logarithmic axis in the frequency range of 0.5 to 20 Hz.

For the RF evaluation, the data for 10.24 s from the first P wave were used. To reduce the errors because a denominator was close to 0, we used the extended-time multitaper technique (Shibutani et al., 2008 [8]). To reduce the effects of scattering, we applied a Gaussian filter that cut values 1 Hz or higher. The ensemble average value of RF for the selected earthquakes was taken as the observed RF. The result is shown in Fig. 3(B).

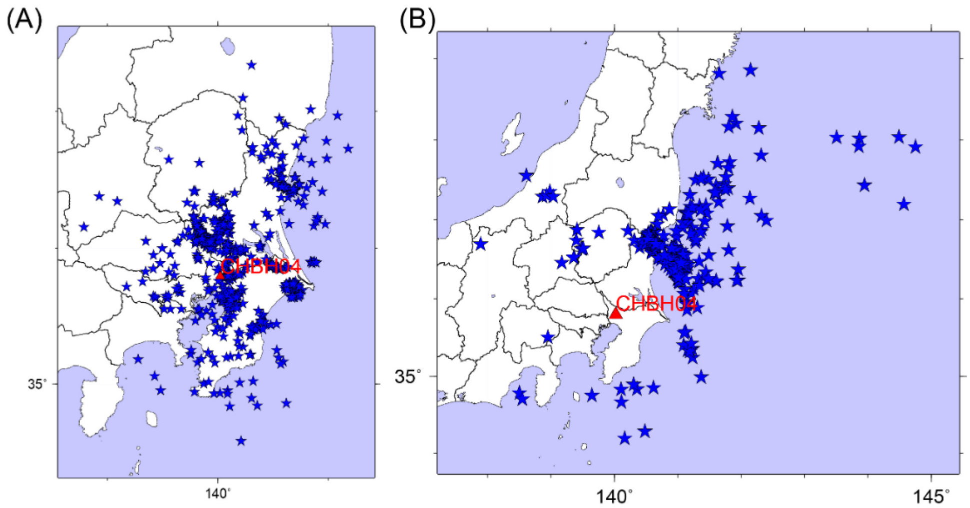

Fig. 2 – The test site for the inversion and the epicenter distribution map used for the evaluations (A: HVSR and B: RF). The earthquake of A is also used for the simulation described later.

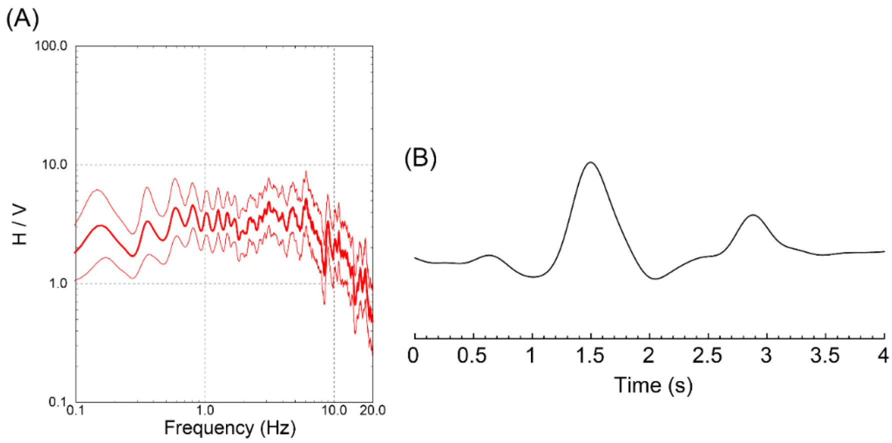

Fig. 3 – HVSR (A) and RF (B) evaluated from the surface observation records of CHBH04. The thick line in (A) represents the average, the thin line represents the average ± standard deviation, and (B) represents the average of RF.

Before the estimation of HVSR and RF, we fixed the orientation of the seismometer at the ground surface by the correlation of the long-term component particle motion with the underground observation point (Kato et al., 2001 [9]). For the orientation of the seismometer at the down hole, we referred to the value evaluated by Shiomi et al. (2003) [10]. The azimuth corrected waveforms were used not only for evaluation of RF and HVSR but also for a simulation of the earthquake motions and a seismic wave interferometry to evaluate a travel time mentioned in section 5.

4. An Inversion of a Subsurface Model

We set a search range, which is shown in Table 1, for inversions with HVSR, RF, and both HVSR and RF. LL and UL stand for lower limit and upper limit, respectively. In the inversions, Vs and Vp were constrained so that Vs and Vp were not lower than those of the upper layer. For Vp in the second layer and deeper, unknown parameters were set deviation rates from the empirical equation between Vs and Vp, which is $Vp = 1.39*Vs + 1189.4$, proposed by Nagashima et al. (2019) [11]. For the damping of the S wave, hs, we used 1% evaluated in advance by seismic interferometry, and for the P wave, hp, we set the ratio to the hs as an unknown parameter. The density was fixed to the value by previous research studies [4, 5]. In an inversion with RF, Ammon et al. (1990) [12] indicated that there is a trade-off between Vs and the layer thickness of the intermediate layer. A similar trade-off is also expected in an inversion with HVSR, because HVSR is not an absolute value but a spectral ratio. Therefore, we fixed the layer thickness and confirmed whether such a trade-off occurred in the inversions.

Table 1 – Search range for an inversion of the subsurface models.

layer	density (t/m^3)	Vs (m/s)		Vp (m/s)		thickness (m)	hs	hp
		LL	UL	LL	UL			
1	1.7	100	240	240	600	3		
2	1.8	170	340	−0.1*	0.1*	9.5		
3	1.8	240	480	−0.1*	0.1*	7		
4	1.9	230	460	−0.1*	0.1*	31.5		
5	1.9	280	460	−0.1*	0.1*	28	0.01	0.5～2.0hs
6	2.0	340	680	−0.1*	0.1*	272		
7	2.1	500	1000	−0.1*	0.1*	497		
8	2.2	630	1260	−0.1*	0.1*	345		
9	2.5	820	1640	−0.1*	0.1*	309		
10	2.7	2540		5000		∞		

Figure 4 shows a comparison of the inverted subsurface models, which is shown with red lines, and PS logging models, with gray lines. Figure 4(A) shows a shallow part up to GL-100 m, and Fig. 4(B) shows a deep part up to GL-2,000 m. At depths less than GL-30 m, the inverted models are in good agreement with the PS logging model, but at depths deeper than GL-30 m, the inverted models appear to be faster than the PS logging model. As one of the reasons for this discrepancy, we considered a constraint that was made so as not to make a low velocity zone (LVZ), and the model near the ground surface contributes more effectively to the HVSRs than the LVZ. In the deep part, shown in Fig. 4(B), the joint model corresponds to the PS logging model. The HVSR model has a higher Vs than the PS logging model, and the RF model has a slightly lower Vs than the PS logging model.

We show a comparison between the theoretical and observed values of HVSRs and RFs by each model in Fig. 5. At this time, we used an S wave damping factor of 1% and a P wave damping factor of the inverted value. The damping of the PS logging model was set to the same value as that of the joint model. In Fig. 5(A), the black line represents the observed value, and the red line represents the theoretical value using the inverted models. Because the adapted frequency range was 0.5 to 20 Hz for the inversions, the peak, seen at 0.1 to 0.2 Hz, did not correspond to any model. However, the shape of the observed HVSR was successfully reproduced by the inverted models, except for the HVSR model.

In the RF comparison of Fig. 5(B), the top waveform shows the observed values, and the second and subsequent waveforms show the theoretical values from each model. The theoretical RF from the HVSR model does not correspond to the observed one, as the peak time of the theoretical one is seen for a shorter time than that of the observed one. We can recognize that the other models have a good reproducibility and that the deep part of the Vs model up to the seismic basement was accurately estimated.

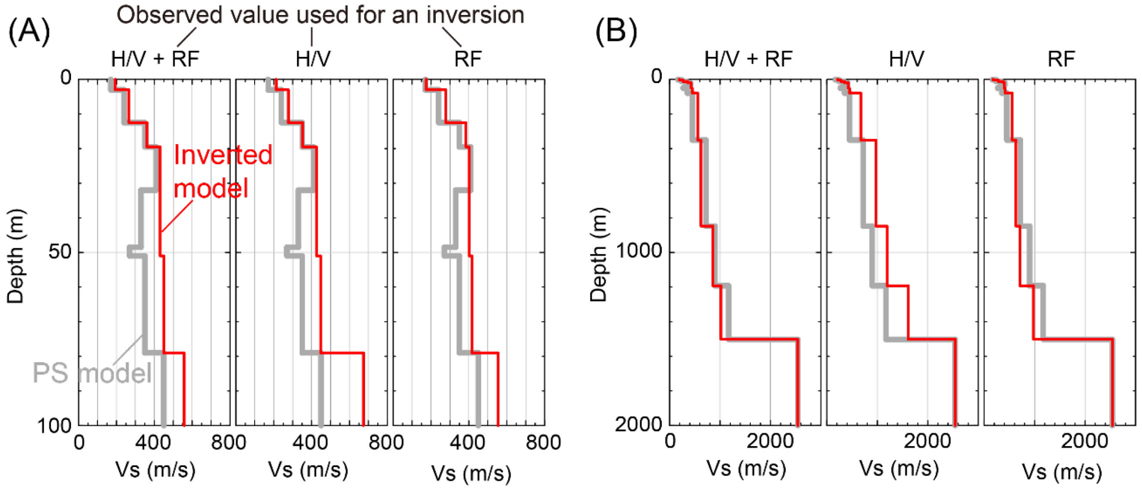

Fig. 4 – Comparison of the Vs profiles of the PS logging model (gray line) with the inverted models (red line) (A: shallow part up to GL-100 m and B: deep part up to GL-2,000 m).

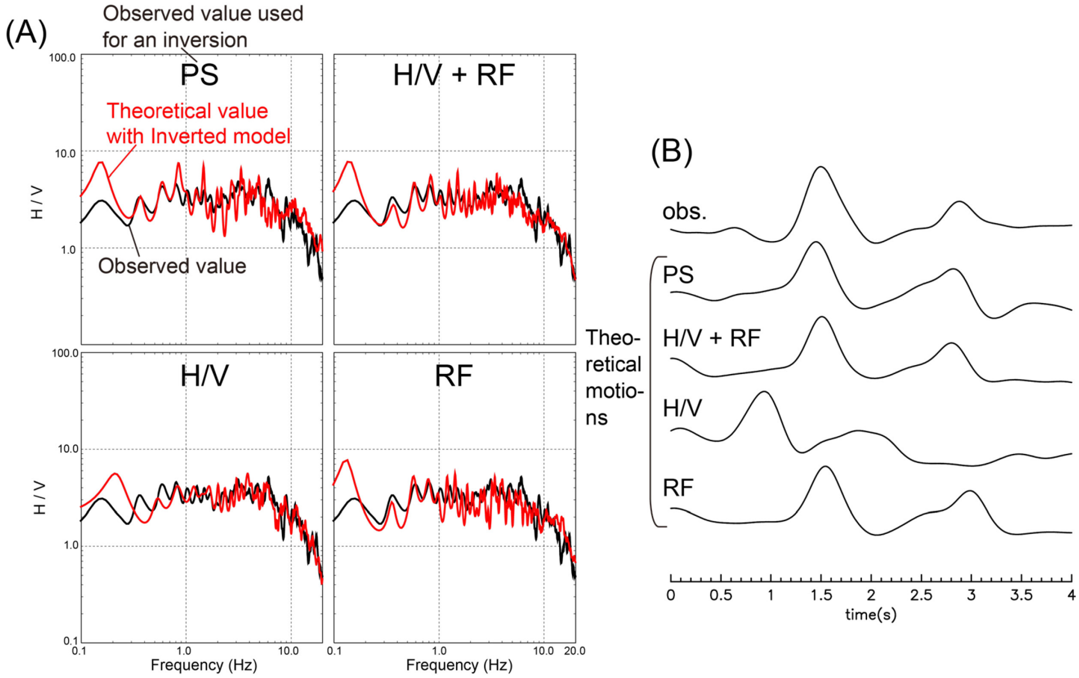

Fig. 5 – Comparison of theoretical and observed values by the inverted model (A: H/V comparison and B: RF comparison).

5. Validation of Models

We used earthquake motions recorded at ground surface and at a depth of 2,500 m as the target in the validation of the subsurface models. When estimating the validity of the models with regard to which of them was appropriate among the three inverted models and the PS logging model, we compared the theoretical value with the observed value as shown in the flowchart in Fig. 6. Goodness of fit (GOF) was verified with two indicators. One was the reproducibility of the response spectra of the simulation for the surface records using the observed motions at the down hole. The other was the reproducibility of the traveling time of the S waves between the stations installed in the vertical array. For the former indication, we simulated the earthquake motions at the ground surface by means of a one-dimensional (1D) wave propagation theory and evaluated GOF between the simulated and observed motions. We adopted GOF as proposed by Anderson (2004) [13]. The GOF of the response spectra means the reproducibility of the amplitude characteristic. For the latter indicator, we evaluated the vertical travel time from the down hole station to the ground level station using seismic interferometry and evaluated the deviation rate from the observed value by comparing the vertical S wave travel times evaluated from each inverted model. We referred to Nakata and Sniedel (2012) [14] for a concrete methodology of an estimation of the deconvolution waveforms. The travel time difference of the S wave between the observed and calculated times mainly indicates the reproducibility of the phase characteristics.

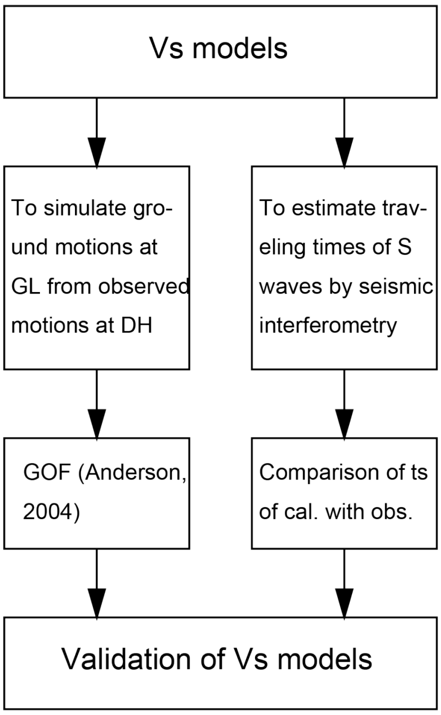

Fig. 6 – Flowchart for examining the validity of the subsurface model.

For the simulation of the ground surface records, we set a target to 768 earthquakes, whose epicenters are shown in Fig. 2(A); these are the same as those for an evaluation of HVSR. Because 1D wave propagation theory was applied for the body waves, it was desirable that the earthquakes occurred near the station with deep hypocenters. Fig. 7(A) shows the distribution of the GOF evaluated for the 1,536 records of the two horizontal components of each earthquake. In the frequency distribution of the GOF, the HVSR model performed slightly better than the other models. For comparison among the models, we evaluated the average value and the ratio of N_{GOF6} to N, where N_{GOF6} is the number of earthquake motions where GOF is equal to or higher than six, and N is the total number of the analyzed earthquake motions as shown in Fig. 7(B) and (C).

The HVSR model is the best from both the average and the ratio aspects. One of the reasons for this is that in the diffusion wave field theory, HVSR is a theory that expresses an amplification factor from a seismic basement (Kawase et al., 2011 [1]). We could say that the HVSR model would effectively reproduce the amplification factor due to the sedimentary layers. The PS logging model was the second best; the joint model was third, with almost the same value as the PS logging model. This suggests that the joint model could successfully reproduce a model equivalent to the PS logging model. The lowest reproducibility was in the RF model. One of the reasons for this is that RF has a low sensitivity for the shallow part, which relates to an amplification factor in a short period range, as shown in Fig. 1.

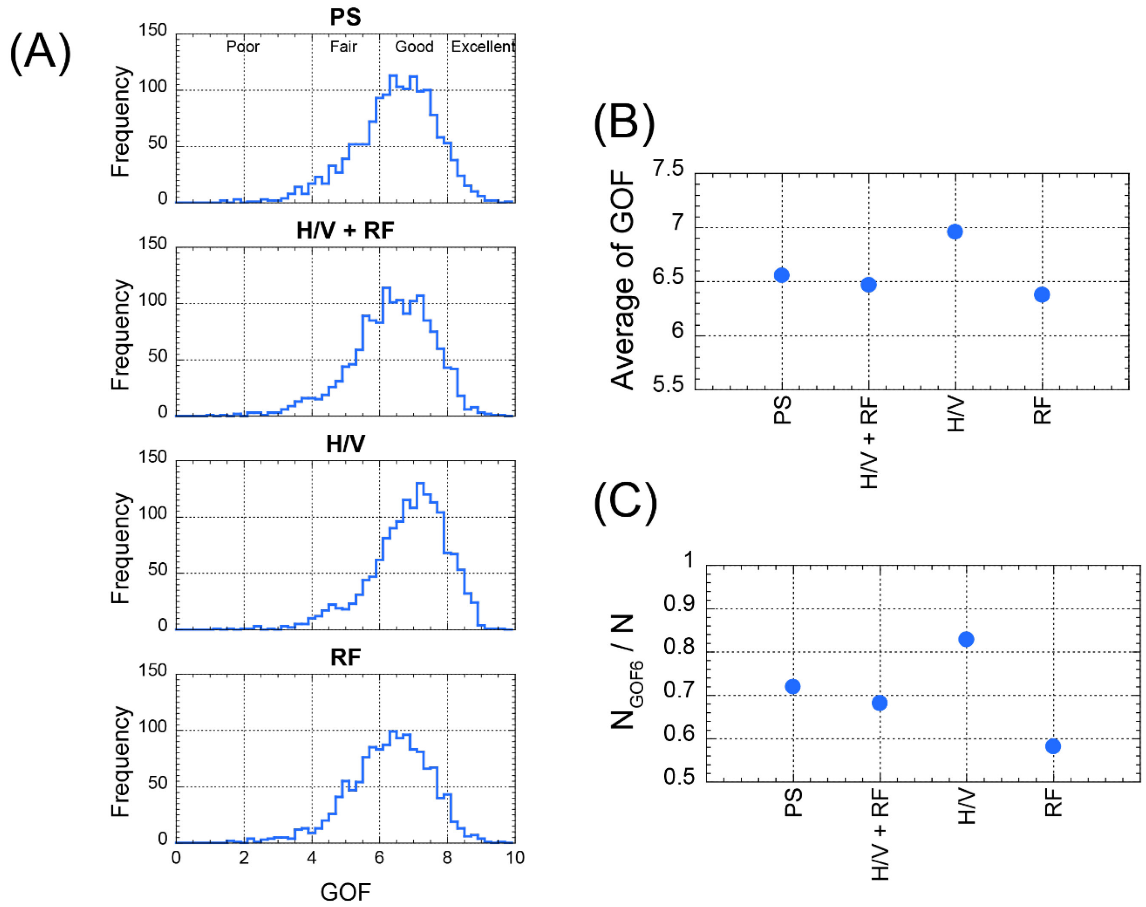

Fig. 7 – GOF distribution of response spectra between the simulated and observed motions at the ground surface using each model (A), average GOF of 1536 waves (B), the ratio of N_{GOF6} to N where N_{GOF6} is the number of earthquake motions where GOF was equal to or higher than six, and N was the total number of the analyzed earthquake motions (C).

Next, we focused on the travel times of the S waves. Fig. 8(A) shows a deconvolution waveform of the motions at the ground surface against those at the down hole. For a precise estimation of the peak time higher than the sampling frequency, we performed a curve fitting technique with a quadratic function and extracted the peak time of the fitted function. We confirmed that the accuracy of a peak time by curve fitting was higher than 0.001 s using a numerical examination. The peak time of the deconvolution waveform was estimated to be 2.437 s. Figure 8(B) shows the value obtained by dividing the residual of the S wave travel time of each model by the observed travel time. The model that was estimated to be closer to 0 was the better model. The PS logging model was estimated to have a residual of approximately 2%, showing the best value. The joint model showed approximately 3%, which could be recognized as equivalent to the PS logging model. The reproducibility of the HVSR model was the worst, with an error of >20%. This could be confirmed from the reproducibility of the first peak frequency of HVSR, as shown in Fig. 5(A), and the reproducibility of RF, as shown in Fig. 5(B). In other words, the reproducibility of the HVSR model for the deep part of a subsurface model is not high; this is because HVSR has a low sensitivity to the deep part, as shown in Fig. 1.

It is worth noting that a model of the joint inversion of HVSR and RF can make a model that is comparable with the PS logging model, from the point of view of reproducibility of the amplification, as shown in Fig. 7(B) and (C), and the travel time, as shown in Fig. 8(B).

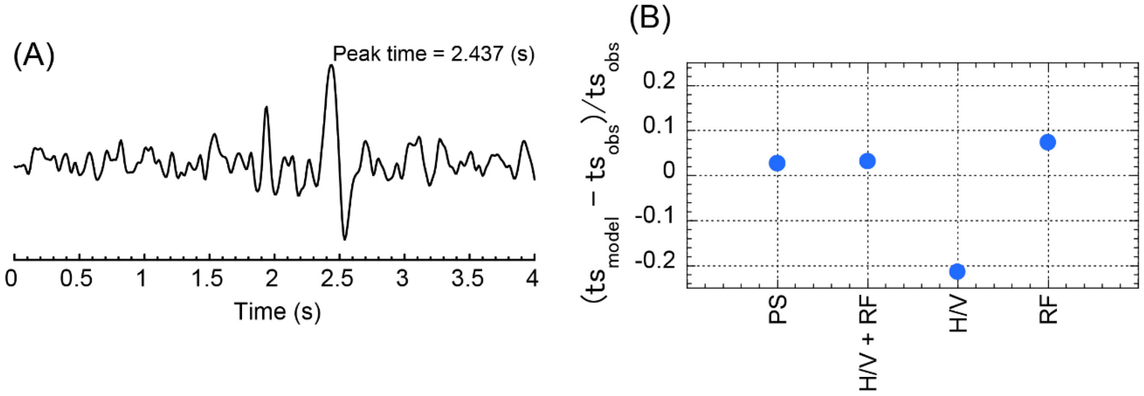

Fig. 8 – A deconvolution waveform of the earthquake motions at the ground surface against those at the down hole (A). The peak time is also shown in (A). Error rates of the travel time of the S wave between the observed time and the calculated time by the inverted models are shown in (B).

Finally, we focused on the sensitivity of the inverted model. With reference to Ammon et al. (1990) [12], the sensitivity indicates how the error is distributed (error surface) when the Vs and the layer thicknesses are varied. Fig. 9 shows the error surfaces for the first layer and the sixth layer. A variation range is set to 50% on both Vs and layer thicknesses. The vertical axis represents the varying layer thicknesses, and the horizontal axis represents the varying Vs. When varying the Vs, Poisson's ratio is fixed. The center represents the inverted model value. For each model, the error was evaluated using the error equations (1), (2), and (3). A white area indicates that the error was quite small. The area became blacker as the error increased. In other words, if the area of the white portion is large, it indicates that there is a possibility that the solution can be taken anywhere for that layer and that the sensitivity for that layer is low. Conversely, when the white area is as narrow as a dot, it indicates that the sensitivity is high for that layer.

The upper right panel of Fig. 9 shows the error surface of the first layer of the RF model and indicates that the white area is large and the sensitivity of RF to the first layer is low, as confirmed in the lower panels of Fig. 1(C). The error surface of the first layer of the joint model, shown in the upper left panel, seems to be a mixture of the RF model and the HVSR model. In other words, by combining the HVSR and RF, the sensitivity becomes high both in a shallow and a deep part of the model, because the HVSR and the RF work well together.

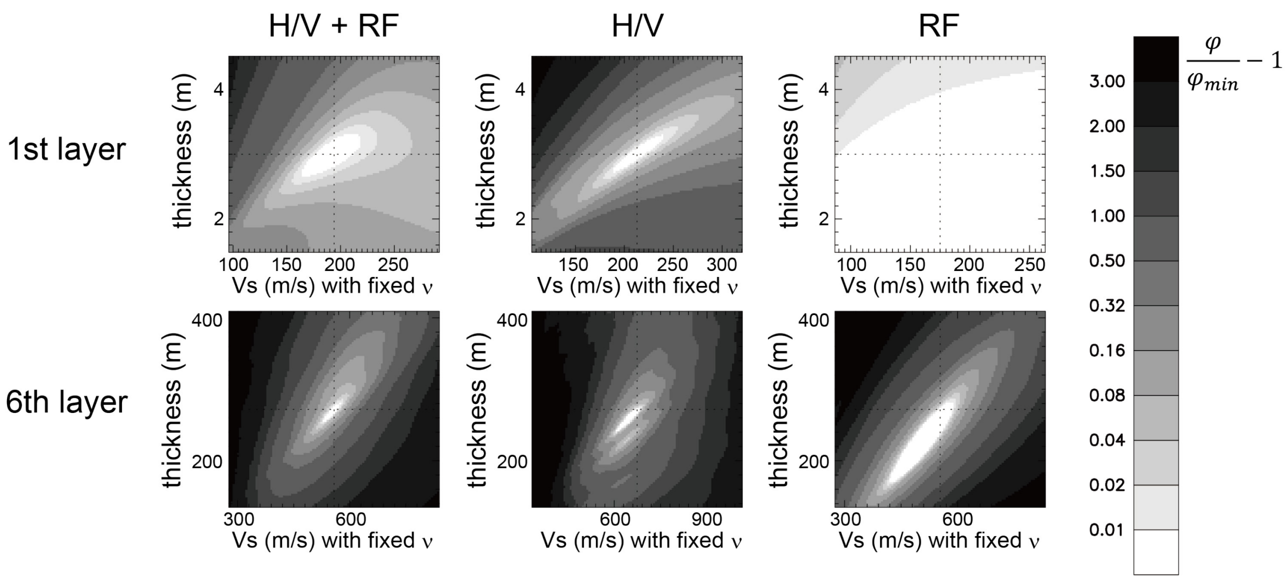

Fig. 9 – Error distribution, varying the Vs and layer thicknesses of the first and sixth layers of the inverted models. When varying the Vs, Poisson's ratio is constant.

In the sensitivity test, we confirmed the trade-off relationship between the layer thicknesses and the Vs. Looking at the error phase of the sixth layer of the RF model, shown in the lower right panel, the white part is spread diagonally. This indicates, as pointed out by Ammon et al. (1990) [12], that there is a trade-off between the layer thicknesses and the Vs and that it is difficult to fix a model uniquely. The white area of the HVSR model is smaller than that of the RF model, but the white area also spreads diagonally. In the joint model, although the multiple local minimum seen in the sixth layer of the HVSR model is resolved, the white area spreads diagonally in the error surface of the first and sixth layers. Therefore, the trade-off between layer thickness and the S wave velocity has not been eliminated, even with a joint inversion. To uniquely construct a subsurface model, we would need to mix other physical quantities, such as the phase velocity or *a priori* information of the thicknesses or Vs.

6. Conclusions

We proposed a joint inversion of HVSR and RF to construct an appropriate subsurface model from the records of a single point on the ground surface. The concluding remarks are shown as follows:

1) We confirmed that HVSR has a high sensitivity in a shallow part of the subsurface model, and RF has a high sensitivity in a deep part. When joined, they act complementarily, and it is possible to construct a model with high sensitivity for both the shallow and deep parts of the models.

2) In the application of joint inversion to a station with a thick sedimentary layer, the inverted model can be constructed comparable with the PS logging model, and it was confirmed that the earthquake motions could be reproduced successfully in both amplitude and phase characteristics with their models.

3) It was confirmed that the trade-off relationship between the layer thickness and the S wave velocity could not be resolved even in the jointed model. It is difficult to find the unique solution from RF and HVSR, and it is necessary to refer to other physical quantities, such as the phase velocity, or obtain *a priori* information of the thickness or S wave velocity, to improve the accuracy.

In this case, we performed the inversion for the observation points with thick sedimentary layers, which could be regarded as the stratified layer. As a next step, we will now investigate the applicability of the joint inversion to stations where the depth of the seismic bedrock is shallow or to stations where layer boundaries can be regarded as being highly irregular.

7. Acknowledgments

As part of the analysis in this study, we used observation records obtained from KiK-net [15]. Some of the source information of the earthquakes was referred to the public information by Hi-net [15]. GMT [16] was used to make some figures. We are grateful to everyone concerned.

8. References

[1] Kawase H, Sanchez-Sesma FJ, Matsushima S (2011): The optimal use of horizontal-to-vertical spectral ratios of earthquake motions for velocity inversions based on diffuse-field theory for plane waves. *BSSA*, **101** (5), 2001-2014.

[2] Langston CA (1979): Structure under Mount Rainier, Washington, inferred from teleseismic body waves. *J. Geophys*. Res., **84** (B9), 4749-4762.

[3] Yamanaka H (2007): Inversion of surface-wave phase velocity using hybrid heuristic search method. *BUTSURI-TANSA*, **60** (3), 265-275. (in Japanese with English abstract).

[4] Ohta Y, Goto N, Yamamizu F, Takahashi H (1980): S-wave velocity measurements in deep soil deposit and bedrock by means of an elaborated down-hole method. *BSSA*, **70** (1), 363-377.

[5] Kinoshita S, Ohike M (2002): Attenuation characteristics of S-wave in a sedimentary layer-basement system in the Kanto region, Japan, for a frequency range of 0.5 to 16 Hz. *J. Seism. Soc. Jpn. (Zisin)*, **55**, 19-31. (in Japanese with English abstract).

[6] Fukushima R, Nakahara H, Nishimura T (2016): Estimating S-wave attenuation in sediments by deconvolution analysis of KiK-net borehole seismograms. *BSSA*, **106** (2), 552-559.

[7] Ueno H, Hatakeyama S, Aketagawa T, Funasaki J, Hamada N (2002): Improvement of hypocenter determination, procedures in the Japan Meteorological Agency. *Quarterly J. of Seism.*, **65**, 123-134. (in Japanese with English abstract)

[8] Shibutani T, Ueno T, Hisahara K (2008): Improvement in the extended-time multitaper receiver function estimation technique. *BSSA*, **98** (2), 812-816.

[9] Kato K, Yamazoe M, Takemura M (2001): Azimuth estimation of KiK-net borehole seismometers distributed in Cyugoku and Shikoku Regions, Japan -On the basis of strong motion records from the Tottoriken-seibu and the Geiyo earthquake-. *J. Seism. Soc. Jpn. (Zisin)*, **54**, 421-429. (in Japanese with English abstract)

[10] Shiomi K, Obara K, Aoi S, Kasahara K (2003): Estimation on the azimuth of the Hi-net and KiK-net borehole seismometers. *J. Seism. Soc. Jpn. (Zisin)*, **56**, 99-110. (in Japanese with English abstract)

[11] Nagashima F, Kawase H (2019): The relationship between Vs, Vp and depth based on PS-logging data at K-NET and KiK-net sites. *BUTSURI-TANSA*, **72**, 78-100. (in Japanese with English abstract).

[12] Ammon CJ, Randall GE, Zandt G (1990): On the non-uniqueness of receiver function inversions. *J. Geophys. Res.,* **95**, 15303-15318.

[13] Anderson JG (2004): Quantitative measure of the goodness-of-fit of synthetic seismograms. *Proceedings of the 13th World Conference on Earthquake Engineering, Vancouver*, B.C., Canada, Paper No. 243.

[14] Nakata N, Snieder R (2012): Estimating near-surface shear-wave velocities in Japan by applying seismic interferometry to KiK-net data. *J. Geophys. Res.*, **117**, B01308.

[15] National Research Institute for Earth Science and Disaster Resilience (2019): NIED K-NET, KiK-net, National Research Institute for Earth Science and Disaster Resilience, doi:10.17598/NIED.0004

[16] Wessel P, Smith WHF (1998): New improved version of Generic Mapping Tools released. *EOS, Trans. AGU*, **79**, 579.

